Linewidth-Optimized Extraordinary Optical Transmission in Water with Template-Stripped Metallic Nanohole Arrays

*Si Hoon Lee, Timothy W. Johnson, Nathan C. Lindquist, Hyungsoon Im, David J. Norris, and Sang-Hyun Oh**

The experimental observation of unusually sharp plasmon resonance peaks in periodic Ag nanohole arrays made using template stripping is reported. The extraordinary optical transmission (EOT) peak associated with the surface plasmon polaritons at the smooth Ag-water interface shows a well-defined Fano-type profile with a linewidth below 10 nm at a wavelength of around 700 nm. Notably, this sharp and intense radiant peak (Q factor of 71) is obtained at visible frequencies in water and at normally incident illumination. This is accomplished by obtaining high-quality Ag surfaces with a roughness below 1 nm, which reduces the imaginary component of the Ag dielectric function that is associated with material damping, as well as shrinking the nanohole radius to decrease radiative damping of plasmons. The localized spectral response of the radiant plasmon peak is characterized using the nanohole array in water in a layer-by-layer fashion via sequential atomic layer deposition of Al_2O_3. Because the ultrasharp EOT peak is obtained with excellent uniformity over a centimeter-sized area from the metallic nanohole array in water, these template-stripped nanohole arrays will benefit many practical applications based on EOT.

1. Introduction

Engineered metallic nanostructures can exhibit unusual optical properties not found in natural materials. With proper design, tuning, and high-throughput fabrication, such metallic nanostructures can be tailored for practical applications such as biosensing, spectroscopy, imaging, and photovoltaics. In particular, following the discovery of extraordinary optical transmission (EOT) through periodic subwavelength hole arrays in metal films,[1] extensive research has been conducted to both understand the physical transmission mechanism[2–5] and to practically produce these nanostructured films with high throughput for emerging applications in plasmonics and nanophotonics.[6–13] In EOT, the excitation of surface plasmon polaritons (SPP) in metallic films leads to a series of optical transmission peaks. The SPP excitation conditions and the peak transmission wavelengths are determined by geometrical parameters (hole size, shape, periodicity, and film thickness) as well as dielectric functions of the metal film and surrounding medium.[5] The far-field EOT peaks exhibit an asymmetric profile described by the Fano-type interference between direct transmission through the holes and the resonant surface modes.[8,14–18]

For many applications in plasmonics, it is desirable to minimize the spectral linewidth to obtain sharp and intense resonance peaks. EOT peaks can be made sharper by reducing the radiative damping of SPPs due to the nanoholes or by reducing the optical losses in the metal. Typically, EOT spectra in the visible regime have been studied using hole diameters ranging from 150 to 300 nm.[5] However, previous work demonstrated that the radiative damping of SPPs increases with the fourth power of the hole size.[19–21] In the near-infrared regime, Tetz et al. demonstrated linewidth reduction by placing gold nanohole arrays between two crossed polarizers to allow only SPP-mediated transmission.[8] Recent work also reported a sharp resonance profile in air by using sub-radiant modes excited at angled illumination.[22] However, sub-radiant modes are much weaker in intensity compared to direct EOT peaks, and the measurements were performed in air. For biosensing, it is desirable to utilize sharp peaks from a "bright" mode in the visible regime while at the same time using nanoholes immersed in water.

To accomplish this, one needs to simultaneously reduce radiative damping by tuning the hole size and minimize the optical losses at visible frequencies by producing extremely high-quality metal films. Since SPPs are tightly bound to the metal interface, they are very sensitive to nanometric geometries–an attribute good for sensing but that also makes SPPs vulnerable to any random surface roughness and grain boundaries in the metal film. Because as-deposited metal films exhibit rough top surfaces, there is often a mismatch between theoretical calculations and measured device performance. A simple technique known as template stripping[23] can resolve this problem and

S. H. Lee, T. W. Johnson, Prof. N. C. Lindquist,[+] Dr. H. Im,[++] Prof. S.-H. Oh
Laboratory of Nanostructures and Biosensing
University of Minnesota
Twin Cities, MN 55455, USA
E-mail: sang@umn.edu
Prof. D. J. Norris
Optical Materials Engineering Laboratory
ETH Zurich, 8092 Zurich, Switzerland
[+] Present address: Physics Department, Bethel University, St. Paul, MN 55122, USA
[++] Present address: Center for Systems Biology, Massachusetts General Hospital, Harvard Medical School, Boston, MA 02114, USA

DOI: 10.1002/adfm.201200955

produce atomically smooth metallic surfaces with improved optical performance. Recently, template stripping has been extended to produce patterned metals, wherein metal films are deposited and subsequently stripped from a reusable patterned silicon template, replicating the smooth interface.[13,24–29] This technique can meet the stringent requirements of reproducible high-throughput fabrication of high-quality metallic nanostructures. Furthermore, along with an improved dielectric function, a substantial increase (5–7×) in the SPP propagation length has been observed in template-stripped Ag films with roughness below 1 nm.[25,30] However, the effect of smooth surfaces and improved dielectric function on the EOT linewidth, which is of considerable importance for the development of practical plasmonic devices, has not yet been investigated.

In this work, we perform extensive 3D computer modeling to determine the parameters for optimizing the EOT linewidths in metallic nanohole arrays in water, and use template stripping to produce size-tunable nanoholes in cm-sized, ultra-smooth Ag films. After optical characterization, the localized spectral response of the template-stripped Ag nanohole array is measured in a layer-by-layer fashion *in water* by atomic layer deposition (ALD) of an Al_2O_3 film, mimicking the molecular absorption process for biosensing. The Q-factor of the linewidth-optimized, template-stripped Ag nanohole arrays is compared with that of other plasmonic sensing platforms and 3D finite-difference time-domain (FDTD) simulations.

2. Results and Discussion

Previously, template stripping has been employed to make nanohole arrays in metal films with a hole size down to 200 nm.[13,25,28] In this work, significant effort was spent to improve the process, reducing a nanohole size further down to ≈100 nm, sharpening the EOT peaks while achieving extremely uniform optical properties across cm-sized metal films, shown in **Figure 1**. A large-area periodic nanohole Si template is first fabricated by a nanoimprint process, followed by reactive ion etching of the SiO_2 hard mask and Si substrate. Since the mold has periodic nanohole array trenches, a high-fidelity periodic plasmonic nanohole array can be replicated with a single metal deposition and peel-off process (Figure 1d). The perforated nanohole-array film is template-stripped with a UV-cured optical epoxy (NOA 61, Norland Products) (Figure 1e,f). During the metal evaporation on the Si template, apertures are naturally formed in the deposited metal film and the aperture size is gradually reduced. Figure 1a shows a schematic of the diameter control with template stripping. The lateral growth of metal can be reduced via increasing the directionality of metal evaporation (e.g., lower chamber pressure, longer source-to-sample distance, and smaller size of the metal source). We tuned these parameters in the metal evaporation chamber to shrink the nanohole size in a controlled manner and obtain a hole size down to 100 nm. Figure 1b shows the scanning electron microscopy (SEM) image of a Si template and template-stripped Ag nanoholes. The measured nanohole diameter in the Si template is 142 ± 7 nm. After a 100 nm thick metal deposition, the diameter of the template-stripped nanohole is reduced to 128 ±

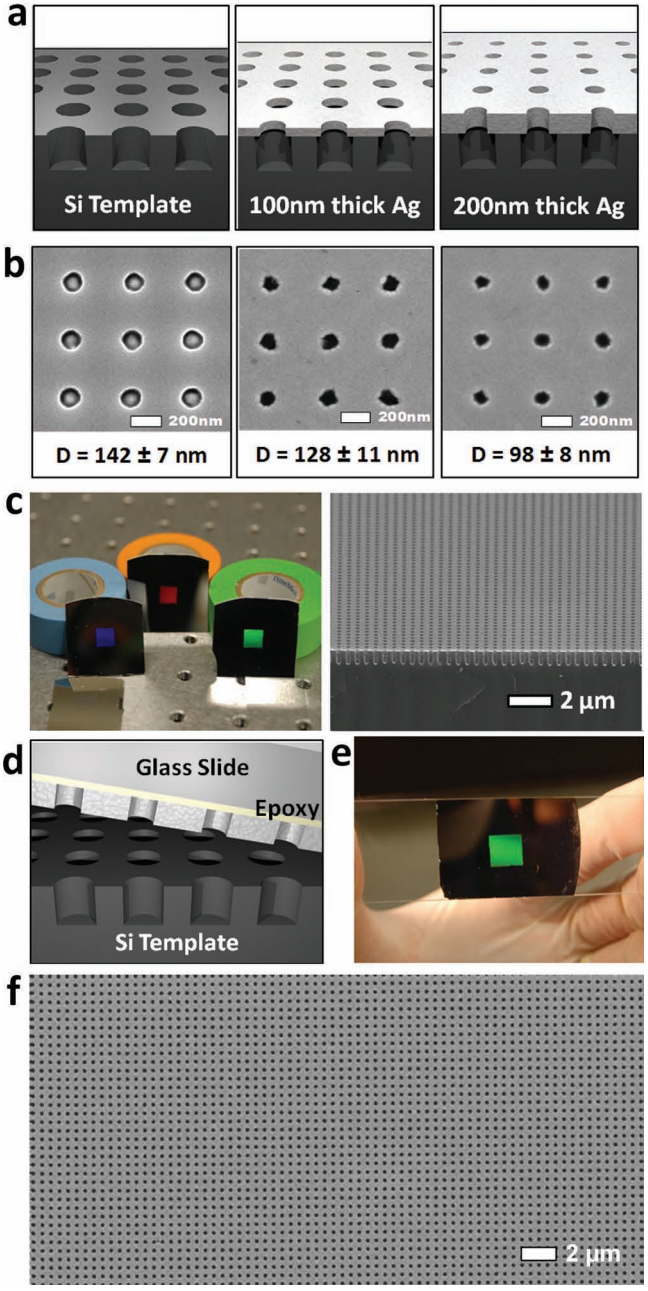

Figure 1. a) Schematic for fabricating size-tunable nanohole arrays in ultra-smooth metallic films via template stripping. As the metal deposition thickness increases, the metal slowly grows laterally, shrinking the hole size. b) A top-down SEM image of the Si template and different thicknesses of template-stripped nanoholes. The measured hole diameter of the mold is 142 ± 7 nm. The hole diameter is reduced to 128 ± 11 nm at a 100 nm thick Ag. The hole diameter is further reduced to 98 ± 8 nm at a 200 nm thick Ag. c) A photograph (left) and a cross-sectional SEM image (right) of the Si nanohole templates after metal deposition. d) Periodic nanohole arrays can be transferred on the glass slide after stripping Ag films using UV-curable epoxy. e) A photograph of an 8 mm × 8 mm area of periodic Ag nanohole arrays fabricated by template stripping shows extremely uniform optical properties over the entire patterned area. f) SEM image of template-stripped Ag periodic nanohole arrays.

11 nm. The diameter is further reduced to 98 ± 8 nm when the film thickness becomes 200 nm. Figure 1c shows a photograph and a cross-sectional SEM of the Si nanohole template after metal deposition.

To elucidate the major factors affecting SPP damping in a nanohole array structure, we simulated the EOT spectra as we varied both the hole diameter from 80 to 200 nm as well as the dielectric functions through 3D FDTD simulations. A commercial software package, FullWave (Rsoft Inc.) was used to perform the simulations. The simulation area contained a single hole with periodic boundaries within the plane of the metal to simulate an infinite array and perfectly matched layer absorbing boundaries in the planes parallel to the metal film. The dielectric functions for the template-stripped Ag films were measured with a VASE (J.A. Wollam Co.) spectroscopic ellipsometer from 250 nm to 1100 nm from a freshly template-stripped sample and numerically fit to a Lorentz-Drude model that was then integrated into the FDTD simulations. As a comparison, we modeled the same structure using dielectric functions obtained from Palik,[31] which are commonly used values for Ag. **Figure 2**b shows the imaginary part of dielectric function of both materials. Notably, the optical loss is reduced significantly in the template-stripped Ag film, as previously shown.[25,30] When the hole diameter is large, the transmission spectra show similar behavior with the two different dielectric functions (d = 200 nm in Figure 2a). This implies that at this diameter range, the transmission peaks are broadened primarily through radiative damping as opposed to material damping. The roughness of the surface becomes important when the diameter approaches ≈150 nm. Asymmetric Fano-type peaks become noticeable in the EOT spectra modeled using template-stripped Ag dielectric functions whereas the spectra modeled using Palik's values show a Lorentzian profile (d = 150 nm in Figure 2a). The spectral positions of the transmission peak maxima at the different grating orders can be approximated with the following equation[2]

$$\lambda_{\max} = a_0 \left[(i^2 + j^2)\right]^{-1/2} \sqrt{\frac{\varepsilon_d \varepsilon_m}{\varepsilon_d + \varepsilon_m}} \quad (1)$$

where a_0 is the periodicity of the array, the integers (i,j) represent the Bragg resonance orders, and ε_m and ε_d are the dielectric functions of the metal and dielectric, respectively. Compared to the (1,0) resonances, the (1,1) resonances, which have a higher diffraction order and occur at shorter wavelengths, show broader spectral widths. As the hole size is decreased further (d = 100 nm in Figure 2a), an ultrasharp (1,0) resonance peak is observed, which is associated with SPPs at the Ag-water interface. Overall, reducing the hole size shifts the peak transmission wavelengths toward shorter wavelengths (blue shift) as previously shown,[5,17,32,33] and changes the line shape to an asymmetric Fano profile. The position of the transmission minima remain unchanged because they are mainly associated with SPP grating coupling with the periodic array.[34]

The relationship between the spectral linewidth and the nanohole diameter is shown in Figure 2c. The linewidth is determined by measuring the full width at half maximum (FWHM) of the (1,0) peak at the Ag-water interface. With a

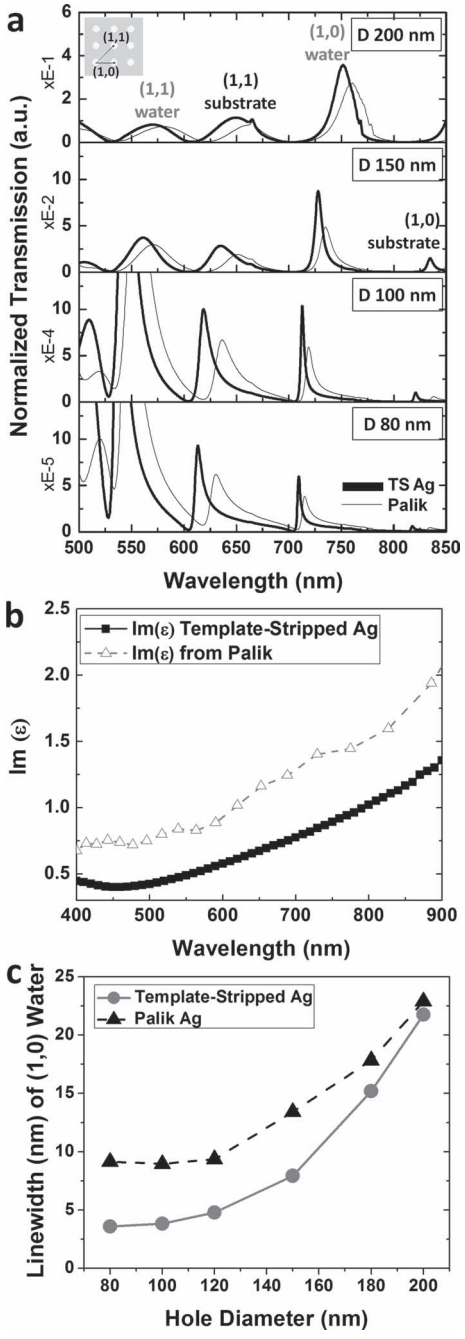

Figure 2. a) 3D FDTD transmission spectra of a nanohole array with varying hole diameter and dielectric functions. Hole diameters (D) are changed from 80 to 200 nm while the periodicity and Ag thickness are maintained at 500 and 200 nm, respectively. The transmission spectra based on the measured dielectric functions of template-stripped Ag are denoted by the thick solid lines and the transmission spectra based on optical constants from Palik are denoted by the thin solid lines.[31] All simulations are performed in a water environment (refractive index value 1.33) with the Ag film attached to an optical epoxy substrate (refractive index value 1.56). b) The imaginary part of the dielectric function used in the 3D FDTD simulation before being fit to a Lorentz-Drude model. The dielectric function of the template-stripped Ag film was measured via ellipsometer. c) Spectral linewidth at the (1,0) resonance versus the hole diameter. The linewidth is FWHM determined from the FDTD spectra.

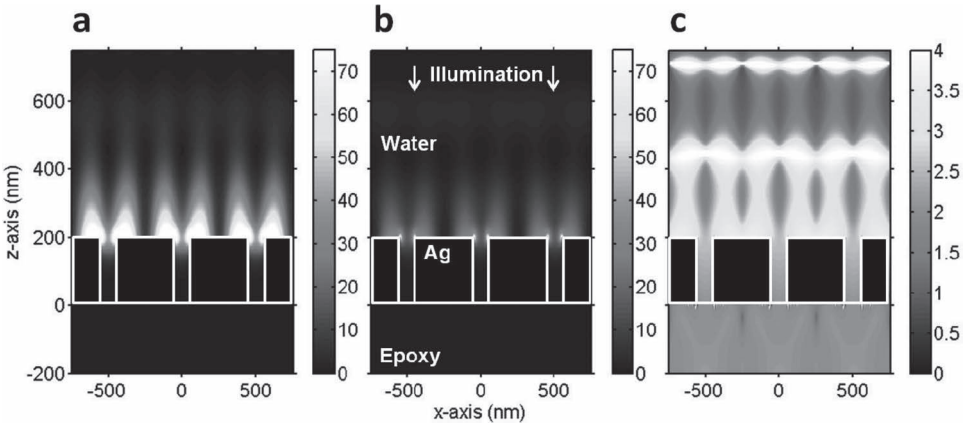

Figure 3. FDTD simulations of the full-field intensity distributions at the peak of the (1,0) water resonance for nanohole arrays with period, Ag thickness, and hole diameters of 500 nm, 200 nm, and 100 nm, respectively, using dielectric functions from a) the template-stripped Ag and b) Palik.[31] The significant increase in field intensity is further emphasized in (c), which shows the field enhancement between (a) and (b) (i.e., panel (a) divided by panel (b)) and indicates both increased transmission and a longer plasmon lifetime.

nanohole diameter of 200 nm, the linewidths from the two different dielectric functions are similar. When the diameter decreases, internal damping, in our case due to excess roughness of the metal surface, starts to emerge as a primary loss mechanism. Upon further reduction of the diameter below ≈120 nm, both linewidths start converging to minimum values but show a considerable difference (FWHM = 3.8 and 9.0 nm from using our experimentally measured template-stripped Ag dielectric functions and those obtained from Palik,[31] respectively).

To further investigate the difference the dielectric functions make, FDTD simulations were done showing the full-field intensity distributions at the various resonances. **Figure 3**a,b show the calculated field intensity for the nanohole arrays using dielectric functions measured from template-stripped Ag films vs. Palik's at the (1,0) resonance (713.3 and 719 nm), respectively. The period of 500 nm, Ag thickness of 200 nm, and hole diameter of 100 nm are maintained the same. The field intensity is much stronger for the case of the measured, template-stripped dielectric functions (Figure 3a) and the enhancement of the smooth, template-stripped Ag nanohole arrays is clearly seen in Figure 3c. The field intensity is enhanced about 2× on the transmission side of the nanohole array which corresponds to the ≈2× increase in transmission of that peak shown (d = 100 nm in Figure 2a). On the incident light side of the nanohole array there is up to a 4x enhancement in the field intensity, which indicates a longer plasmon lifetime in the template-stripped Ag film.

Figure 4a shows the optical transmission spectra measured from a 200 nm-thick template-stripped Ag nanohole array having a 100 nm hole diameter and a 500 nm periodicity. Through extensive device fabrication and FDTD simulations, we performed systematic studies of the various parameters by varying the metallic film thickness (100–200 nm), the substrate index (1.6–2.5, FDTD only), and the array periodicity (500–600 nm). An array periodicity of 500 nm was chosen to position the (1,0) peak in water in the visible regime, close to 700 nm. A film thickness of 200 nm was chosen to have an optically thick Ag film while also reducing the hole size. The index of the substrate (experimentally set by the choice of template stripping epoxy, n = 1.56) was chosen such that the EOT peaks associated with the substrate and water sides are clearly separated, which is required for biosensing as well as investigation of EOT linewidth reduction via template stripping. The measurement was performed after applying a drop of water on the nanohole array and covering it with a glass cover slip. A tungsten-halogen light source illuminated the top surface of the nanohole array through a microscope objective (4×, NA = 0.13) and the directly transmitted light was collected by a fiber-optic spectrometer (Ocean Optics, USB-4000). A 3-D FDTD simulation with the same geometric parameters is compared to the measured data in Figure 4a. The λ_{max} of the (1,0) and (1,1) SP resonances on the water-side of the film, where the surface is the smooth, template-stripped Ag (Figure 4b) show close agreement between experiment and the simulation. However, the peak positions of the substrate (epoxy) side resonances deviate more from the simulations and show broader linewidths, i.e., increased SPP losses, which is likely due to the nominal roughness of the top-side of the evaporated Ag film (Figure 4c). When the hole diameter and metal surface are optimized, very sharp SPP resonance peaks in template-stripped periodic Ag nanohole arrays are observed experimentally. The FWHM of the (1,0) SP resonance in water is measured to be 9.9 nm, and the simulated value is 3.8 nm. The discrepancy is likely due to the finite NA (0.13) of the objective used for illumination and the residual roughness on the nanohole sidewalls formed during metal evaporation. The improvement in plasmon lifetime in nanohole arrays can also be characterized using the measured linewidth relative to the resonance wavelength (the Q factor). According to this definition, the Q factor measured from the (1,0) peak in water is 71, which is among the best values reported in water for visible wavelengths, and indicates a longer SPP lifetime or propagation length on template-stripped Ag surfaces. While it was previously shown that angled illumination of nanohole arrays can sharpen the transmission or reflection peaks,[22,35,36] the fact that we observe a high Q factor at simple normal incidence further reflects a long SPP propagation length from the improved dielectric functions of the metal film.

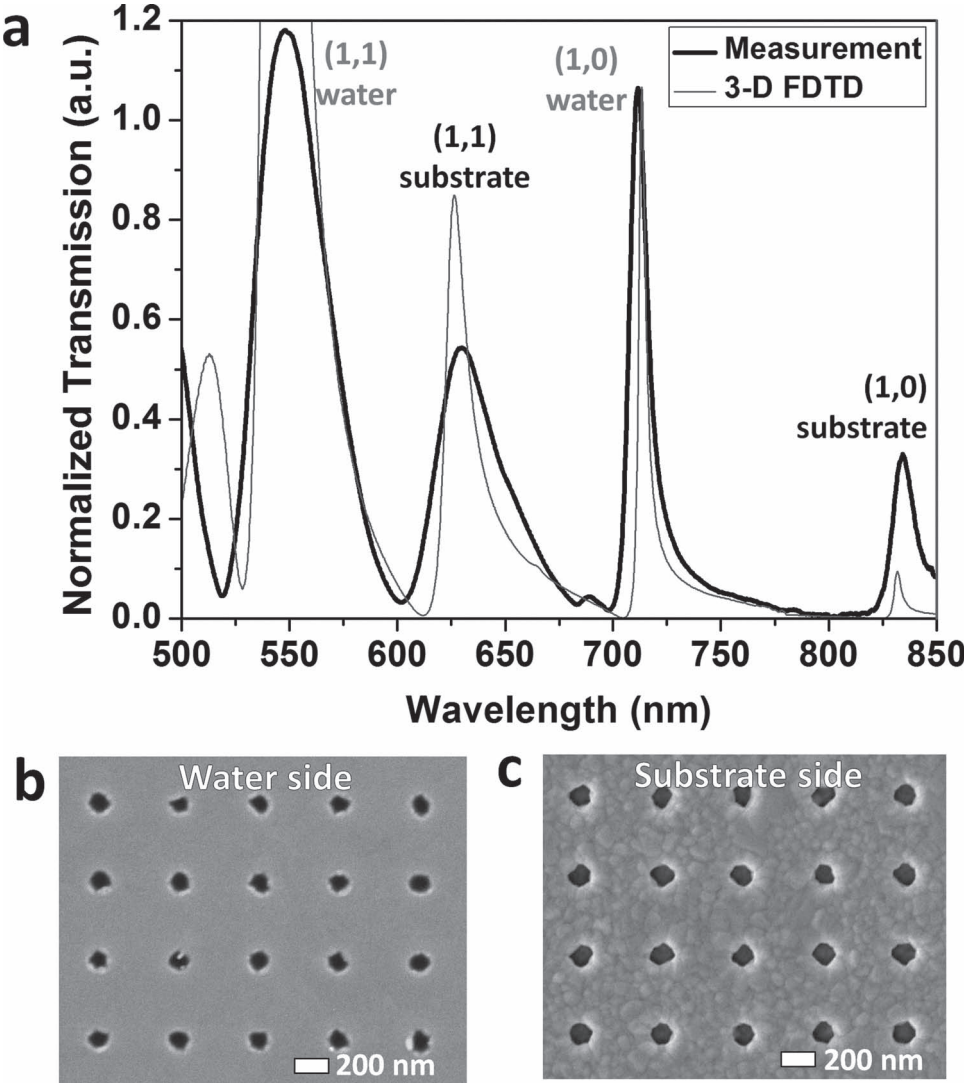

Figure 4. a) Optical transmission spectra of template-stripped nanohole arrays with a 100 nm hole diameter and 500 nm periodicity in a 200 nm-thick Ag film obtained experimentally (thick solid line) and from 3-D FDTD simulation (thin solid line). The spectral linewidths of the (1,0) plasmon peak in water are 9.9 nm and 3.8 nm and Q-factors of these major peaks are 71 and 189 in the measured data and the FDTD simulation, respectively. b) A SEM image of a water-side nanohole array which is the smooth, template-stripped Ag film. c) A SEM image of a substrate-side nanohole array, which is the rough topside of an evaporated Ag film.

To characterize the device sensitivity for biosensing applications, we measured the bulk refractive index sensitivity as well as localized sensitivity for thin-film adsorption. The bulk refractive index sensitivity of the device is measured by injecting solutions with varying values of refractive index over the nanohole arrays using a microfluidic channel. The index-calibrated solution is prepared by varying the amount of glycerol mixed with water and confirmed by a refractometer (Refracto 30PX, Mettler Toledo). **Figure 5**a shows the transmission spectra change as the refractive index solution changes in the 3D FDTD (top) and the experiment (bottom), respectively. The transmission peaks due to SPPs on the Ag-epoxy interface remain unchanged throughout the experiments. The bulk refractive index sensitivity, evaluated from the shift of peak wavelength over the change of refractive index unit (RIU), is presented in Figure 5b. The measured (1,0) bulk sensitivity is 494 nm/RIU, which is slightly lower than the theoretical values based on FDTD simulations (524 nm/RIU). Experimentally, figure of merits (FOM) as high as 50 (495 nm/RIU divided by 9.9 nm) in the visible regime and in water are obtained from the template-stripped nanohole arrays.

While the bulk index sensitivity is straightforward to measure and provides a means to compare the performance of various optical biosensors, the ultimate performance of these sensors is determined by the signal changes resulting from thin-film adsorption, i.e. localized surface sensitivity, since molecular binding events occur within tens of nanometers from the sensing surface. To quantify this local detection sensitivity,

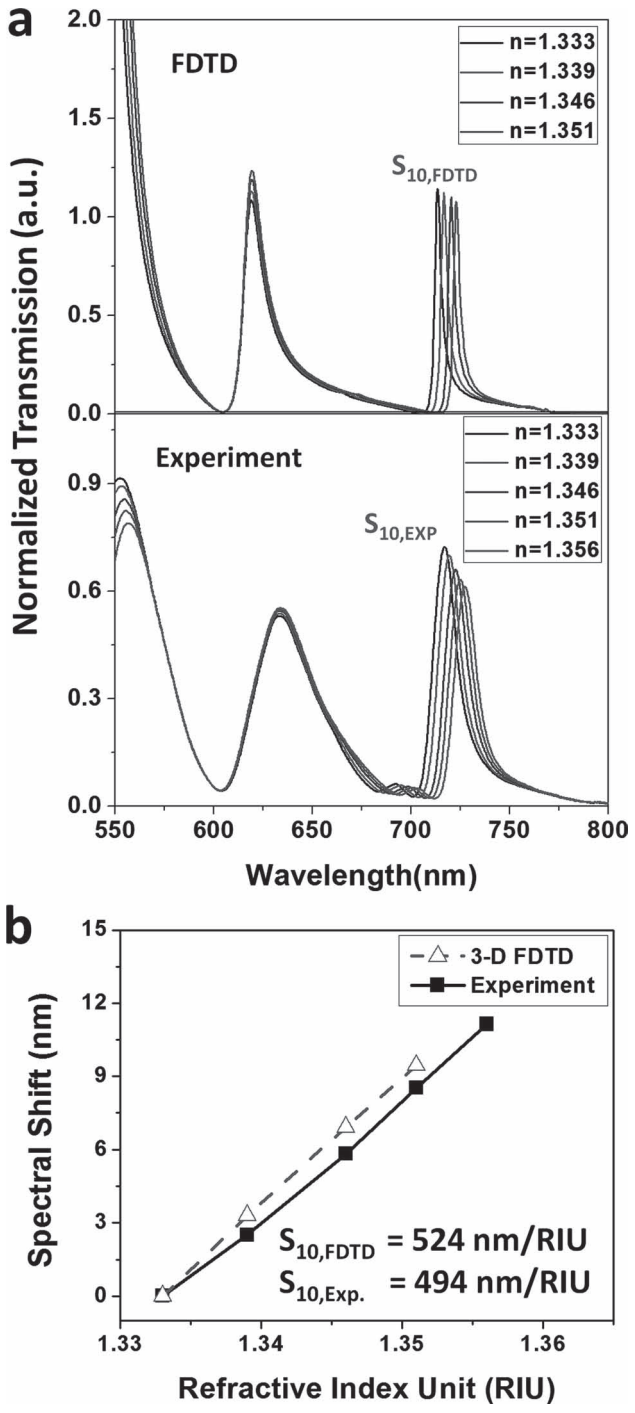

Figure 5. a) The transmission spectra of linewidth-optimized, template-stripped Ag nanohole arrays in index-calibrated water-glycerol solutions. 3D FDTD simulation results (top) are compared with measured optical transmission spectra (bottom). b) The spectral shifts are measured by changing the refractive index of water-glycerol mixture from 1.333 to 1.356. The sensitivities of the (1,0) water SP resonance (S_{10}) are measured from the spectral shifts of the maximum peak position.

ALD of Al_2O_3 has been used for layer-by-layer characterization of the spectral shifts. Previously, such layer-by-layer ALD characterization has been performed in air,[37,38] but the plasmon decay length and local sensitivity will change when the sensor is immersed in water. Therefore, we developed new procedures to measure EOT spectra in water between each successive ALD deposition.

Figure 6a shows a schematic of the local sensitivity measurement of template-stripped Ag nanohole arrays by an ALD process. The spectral shifts of the (1,0) peak are monitored with increasing ALD thickness from 0 to 35 nm in 5 nm intervals. To prevent surface oxidation of Ag, an initial 2 nm of Al_2O_3 layer is formed prior to the first measurement in water. The aqueous condition is maintained during the measurement by using a cover slide after applying a drop of water on the nanohole array. Afterwards, the sample is completely dried with a high purity N_2 before immediately proceeding to the next ALD step. The ALD process is monitored after each interval by ellipsometric measurements on the thickness of the Al_2O_3 deposited on a Si chip processed in the same chamber. While this characterization method is very time-consuming and requires careful sample handling to avoid contamination

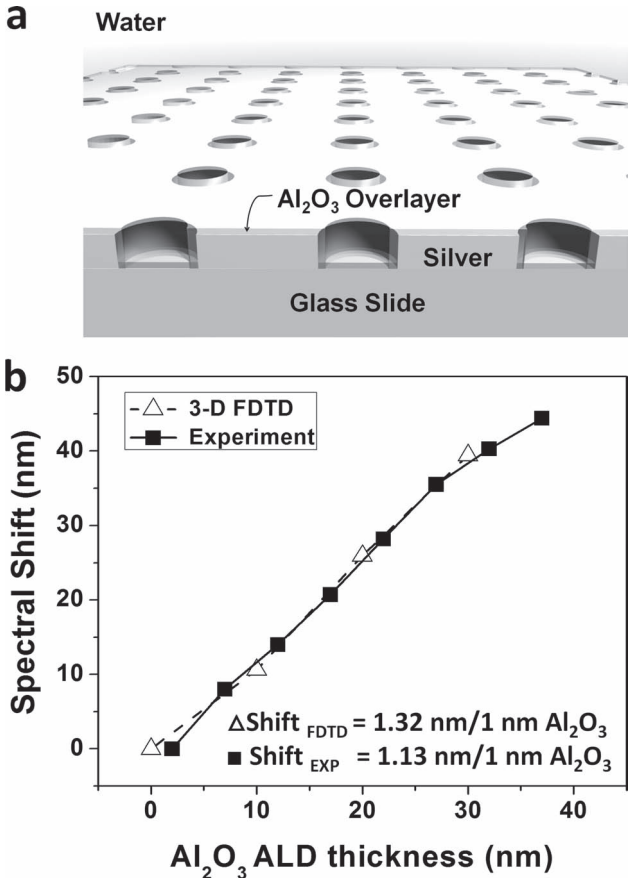

Figure 6. a) A schematic for a local sensitivity measurement of template-stripped nanohole arrays by an Al_2O_3 atomic layer deposition (ALD) process. b) The spectra shifts of (1,0) water SP resonance peaks are measured by increasing ALD thickness. The result of FDTD (triangle, dashed line) matches very well with that of experiment (square, solid line). ALD intervals are 5 nm. The initial 2 nm of Al_2O_3 is deposited to protect the Ag surface from the oxidation of an aqueous environment.

and artifacts, the results obtained are more representative of what one would expect from biosensing in an aqueous environment. FDTD simulations were also carried out adding conformal layers with an index of 1.65 to the surface and in the holes. The local sensitivity of the (1,0) SP resonance peak of Ag nanohole arrays is 1.13 nm shift per 1 nm Al_2O_3, which shows good agreement with the FDTD result (1.32 nm shift per 1 nm Al_2O_3 in Figure 6b). In addition, the spectral shift increases linearly within the ALD thickness range used. Since the ALD process is highly reproducible, this surface sensitivity data obtained in water can help evaluate the local sensitivity of various SPR and LSPR biosensors in practical biosensing environments.

3. Conclusions

We have obtained unusually sharp EOT peaks in water by using template-stripped periodic Ag nanohole arrays with optimized parameters, thereby reducing the materials damping as well as radiative damping. Besides being a massively parallel method to create high-quality metallic nanostructures, the template-stripping process also provides tunability for the nanohole diameter. When the nanohole size is above ≈200 nm, the linewidth at visible frequencies is predominantly determined by the radiative scattering of SPPs by the large nanoholes. Below ≈150 nm nanohole size, materials loss dominates the linewidth, and smooth Ag films can further sharpen the EOT peaks in that regime. We then determined the parameters to optimize the EOT linewidth. The measured linewidth from nanoholes immersed in water is less than 10 nm, among one of the sharpest radiant peaks demonstrated in water. Furthermore, the measured Q-factor of the EOT peak in template-stripped nanohole arrays is as high as 71 at visible frequencies in aqueous conditions. Bulk and local sensitivity of this template-stripped device are in good agreement with the theoretical results (FDTD). Since this sharp peak (9.9 nm linewidth) can be obtained from the cm-sized nanohole array with simple normal incidence illumination via an incoherent light source, it will benefit broad applications based on EOT such as surface plasmon resonance imaging[11,39–42] and spectroscopy.[43–46]

4. Experimental Section

Si Template Fabrication: A NXR-1025 nanoimprint resist (Nanonex Corp., NJ USA) was spin-coated on a Si chip (1 × 1 inch) with 200 nm-thick thermally grown SiO_2 at 3500 r.p.m. for 60 s and cured at 150 °C for 1 min. To prevent sticking, (heptadecafluoro-1,1,2,2-tetrahydrodecyl)trichlorosilane (Gelest Inc, Morrisville, PA USA) was coated on the nanoimprint Si stamp for 12 h prior to the imprinting. After placing the stamp on the resist-coated Si chip, imprinting was performed with a pressure of 300 psi for 2 min at 130 °C. The oxide hard mask was patterned by reactive ion etching (RIE, STS model 320) with 25 sccm of CF_4 and 50 sccm of Ar gases at 150 W for 8 min and 30 s. After removing the residual resist at 100 W for 5 min by oxygen plasma ashing, the periodic nanohole Si template was made by reactive ion etching (Plasma Therm SLR-770). The patterned Si mold was cleaned in a 1:1 mixture of sulfuric acid and hydrogen peroxide for 10 min and the remaining SiO_2 was removed by a buffered oxide etchant (BOE) solution. The mold was then cleaned again in a 1:1 mixture of sulfuric acid and hydrogen peroxide for 10 min and rinsed with DI water.

Metal Deposition and Template Stripping: An e-beam evaporator was used to deposit 100 or 200 nm-thick Ag films onto the Si mold. The initial 20 nm was deposited at 0.2 Å/s. Then, the deposition rate was increased to 1 Å/s for the rest of the thickness. After metal deposition, a UV-curable optical epoxy (NOA 61, Norland Inc., Cranbury, NJ) was applied and cured for 30 min under UV light before template stripping.

Microfluidics: The microfluidic flow cell was fabricated by soft lithography with polydimethylsiloxane (PDMS). SU-8 50 (Microchem) negative photoresist was spin coated on a 4-in. Si wafer at 2000 rpm for 30 s and cured at 65 °C for 6 min and 95 °C for 20 min. Soft-cured SU-8 resist was exposed through a Cr-on-glass photomask using a Karl Suss MA6 mask aligner. Post exposure bake was done at 65 °C for 1 min and 95 °C for 5 min. The resist was developed for 6 min in SU-8 developer. After applying an anti-sticking coating (heptadecafluoro-1,1,2,2-tetrahydrodecyl)trichlorosilane (Gelest Inc, Morrisville, PA USA) on the SU-8 mold, PDMS resin was poured and cured at 60 °C overnight. The microfluidic device used in the refractive index sensing has a single channel with a 50 μm height and a 1000 μm width.

Refractive Index Sensing: Various index-calibrated water-glycerol solutions were made by adding glycerol into the DI water and confirmed by a refractometer (Refracto 30PX, Mettler Toledo). Real-time spectra shifts were measured with a temporal resolution of 2 s (500 ms integration time and 4 times averaging). Different index solutions were injected through a microfluidic flow cell sequentially by using a syringe pump (Harvard Apparatus).

Atomic Layer Deposition: To evaluate the local detection sensitivity of the template-stripped nanohole array device, atomic layer deposition (ALD, Savannah, Cambridge Nanotech) of Al_2O_3 was used for layer-by-layer characterization of spectral shifts. Conformal Al_2O_3 layers are formed by alternately pulsing trimethylaluminum ($Al(CH_3)_3$) and water (H_2O) vapor above the heated (50°C) substrate. The spectral measurements were then taken as described above. Afterwards, the sample is dried with a high purity N_2 before the next ALD step.

Computer Simulations: FDTD simulations were done using a commercial software package, FullWave (Rsoft Inc.). The simulation area contained a single hole with periodic boundaries within the plane of the metal to simulate an infinite array and perfectly matched layer absorbing boundaries in the planes parallel to the metal film. A nominal grid size of 10 nm was used which was graded down to 3 nm within plane of the metal and down to 5 nm in the z-dimension. For the simulations with ALD overlayers the minimum grid size was shrunk to always be at most one tenth of the thickness of the ALD layer (i.e., 1 nm grid in all three dimensions for the simulation with 10 nm of ALD). The refractive indices for the ALD overlayers and epoxy substrate set to 1.65 and 1.56 respectively. The dielectric functions for the metals were numerically fit to a Drude-Lorentz model to be used in the computation.

Acknowledgements

The authors thank Thomas Ebbesen for helpful discussions and comments. This work was supported by grants from the Office of Naval Research (ONR) Young Investigator Award (N00014-11-1-0645) and the NSF CAREER Award (S.-H.O.). This work used resources at the University of Minnesota, including the Nanofabrication Center, which receives partial support from NSF through the National Nanotechnology Infrastructure Network program, and the Characterization Facility, which has received capital equipment funding from NSF through the Materials Research Science and Engineering Center (MRSEC). S.H.L. acknowledges support from a Samsung Fellowship.

Received: April 4, 2012
Published online: July 3, 2012

[1] T. W. Ebbesen, H. J. Lezec, H. F. Ghaemi, T. Thio, P. Wolff, *Nature* **1998**, *391*, 667.
[2] L. Martín-Moreno, F. J. García-Vidal, H. J. Lezec, K. Pellerin, T. Thio, J. B. Pendry, T. W. Ebbesen, *Phys. Rev. Lett.* **2001**, *86*, 1114.
[3] A. Krishnan, T. Thio, T. Kim, H. J. Lezec, T. W. Ebbesen, P. Wolff, J. B. Pendry, L. Martín-Moreno, F. J. García-Vidal, *Opt. Commun.* **2001**, *200*, 1.
[4] C. Genet, T. W. Ebbesen, *Nature* **2007**, *445*, 39.
[5] F. J. García-Vidal, T. W. Ebbesen, L. Kuipers, *Rev. Mod. Phys.* **2010**, *82*, 729.
[6] W. Fan, S. Zhang, B. Minhas, K. Malloy, S. Brueck, *Phys. Rev. Lett.* **2005**, *94*, 033902.
[7] M. E. Stewart, N. H. Mack, V. Malyarchuk, J. A. N. T. Soares, T. W. Lee, S. K. Gray, R. G. Nuzzo, J. A. Rogers, *Proc. Natl. Acad. Sci. USA* **2006**, *103*, 17143.
[8] K. Tetz, L. Pang, Y. Fainman, *Opt. Lett.* **2006**, *31*, 1528.
[9] J. Henzie, M. H. Lee, T. W. Odom, *Nat. Nanotechnol.* **2007**, *2*, 549.
[10] J. Chen, J. Shi, D. Decanini, E. Cambril, Y. Chen, A. M. Haghiri-Gosnet, *Microelectron. Eng.* **2009**, *86*, 632.
[11] J. W. Menezes, J. Ferreira, M. J. L. Santos, L. Cescato, A. G. Brolo, *Adv. Funct. Mater.* **2010**, *20*, 3918.
[12] J. F. Masson, M.-P. Murray-Methot, L. S. Live, *Analyst* **2010**, *135*, 1483.
[13] H. Im, S. H. Lee, N. J. Wittenberg, T. W. Johnson, N. C. Lindquist, P. Nagpal, D. J. Norris, S.-H. Oh, *ACS Nano* **2011**, *5*, 6244.
[14] C. Genet, M. P. van Exter, J. P. Woerdman, *Opt. Commun.* **2003**, *225*, 331.
[15] M. Sarrazin, J.-P. Vigneron, J.-M. Vigoureux, *Phys. Rev. B* **2003**, *67*, 085415.
[16] S. H. Chang, S. K. Gray, G. C. Schatz, *Opt. Express* **2005**, *13*, 3150.
[17] F. J. G. de Ajajo, *Rev. Mod. Phys.* **2007**, *79*, 1267.
[18] B. Luk'yanchuk, N. I. Zheludev, S. A. Maier, N. J. Halas, P. Nordlander, H. Giessen, C. T. Chong, *Nat. Mater.* **2010**, *9*, 707.
[19] D. Kim, S. Hohng, V. Malyarchuk, Y. Yoon, Y. Ahn, K. Yee, J. Park, J. Kim, Q. H. Park, C. Lienau, *Phys. Rev. Lett.* **2003**, *91*, 143901.
[20] R. Muller, V. Malyarchuk, C. Lienau, *Phys. Rev. B* **2003**, *68*, 205415.
[21] F. Przybilla, A. Degiron, C. Genet, T. W. Ebbesen, F. de Leon-Perez, J. Bravo-Abad, F. J. García-Vidal, L. Martín-Moreno, *Opt. Express* **2008**, *16*, 9571.
[22] A. A. Yanik, A. E. Cetin, M. Huang, A. Artar, S. H. Mousavi, A. Khanikaev, J. H. Connor, G. Shvets, H. Altug, *Proc. Natl. Acad. Sci. USA* **2011**, *108*, 11784.
[23] M. Hegner, P. Wagner, G. Semenza, *Surf. Sci.* **1993**, *291*, 39.
[24] C.-H. Sun, N. C. Linn, P. Jiang, *Chem. Mater.* **2007**, *19*, 4551.
[25] P. Nagpal, N. C. Lindquist, S.-H. Oh, D. J. Norris, *Science* **2009**, *325*, 594.
[26] N. C. Lindquist, P. Nagpal, A. Lesuffleur, D. J. Norris, S.-H. Oh, *Nano Lett.* **2010**, *10*, 1369.
[27] J.-C. Yang, H. Gao, J. Y. Suh, W. Zhou, M. H. Lee, T. W. Odom, *Nano Lett.* **2010**, *10*, 3173.
[28] N. C. Lindquist, T. W. Johnson, D. J. Norris, S.-H. Oh, *Nano Lett.* **2011**, *11*, 3526.
[29] N. C. Lindquist, P. Nagpal, K. M. McPeak, D. J. Norris, S.-H. Oh, *Rep. Prog. Phys.* **2012**, *75*, 036501.
[30] J. H. Park, P. Nagpal, S.-H. Oh, D. J. Norris, *Appl. Phys. Lett.* **2012**, *100*, 081105.
[31] E. Palik, *Handbook of Optical Constants of Solids*, Academic, New York **1985**.
[32] K. L. van der Molen, F. B. Segerink, N. F. van Hulst, L. Kuipers, *Appl. Phys. Lett.* **2004**, *85*, 4316.
[33] M.-P. Murray-Methot, M. Ratel, J.-F. Masson, *J. Phys. Chem. C* **2010**, *114*, 8268.
[34] J. M. McMahon, J. Henzie, T. W. Odom, G. C. Schatz, S. K. Gray, *Opt. Express* **2007**, *15*, 18119.
[35] J. Braun, B. Gompf, G. Kobiela, M. Dressel, *Phys. Rev. Lett.* **2009**, *103*, 203901.
[36] H. Gao, J.-C. Yang, J. Y. Lin, A. D. Stuparu, M. H. Lee, M. Mrksich, T. W. Odom, *Nano Lett.* **2010**, *10*, 2549.
[37] A. V. Whitney, J. W. Elam, S. Zou, A. V. Zinovev, C. Peter, G. C. Schatz, R. P. Van Duyne, *J. Phys. Chem. B* **2005**, *109*, 20522.
[38] H. Im, N. C. Lindquist, A. Lesuffleur, S.-H. Oh, *ACS Nano* **2010**, *4*, 947.
[39] A. Lesuffleur, H. Im, N. C. Lindquist, K. S. Lim, S.-H. Oh, *Opt. Express* **2008**, *16*, 219.
[40] J.-C. Yang, J. Ji, J. M. Hogle, D. N. Larson, *Nano Lett.* **2008**, *8*, 2718.
[41] N. C. Lindquist, A. Lesuffleur, H. Im, S.-H. Oh, *Lab Chip* **2009**, *9*, 382.
[42] C. Escobedo, S. Vincent, A. I. K. Choudhury, J. Campbell, A. G. Brolo, D. Sinton, R. Gordon, *J. Micromech. Microeng.* **2011**, *21*, 115001.
[43] A. G. Brolo, E. Arctander, R. Gordon, B. Leathem, K. L. Kavanagh, *Nano Lett.* **2004**, *4*, 2015.
[44] A. G. Brolo, S. C. Kwok, M. G. Moffitt, R. Gordon, J. Riordon, K. L. Kavanagh, *J. Am. Chem. Soc.* **2005**, *127*, 14936.
[45] J. R. Lakowicz, *Anal. Biochem.* **2005**, *337*, 171.
[46] J. A. Hutchison, D. M. O'Carroll, T. Schwartz, C. Genet, T. W. Ebbesen, *Angew. Chem. Int. Ed.* **2011**, *50*, 2085.